2026 IEEE/SICE International Symposium on System Integration (SII)
January 11-14, 2026. Cancún, México

Effects of Continuous Fiber Insertion on the Strength and Stiffness of 3D Printed Parts

Rintaro MATSUSHITA and Yusuke OTA

Abstract—**3D printed parts are widely used, which often require high strength and stiffness. However, 3D printed parts face various challenges, properties for printing materials, continuous fiber orientation, moisture absorption, and printing accuracy. Quantitative evaluation of each of these factors will determine appropriate design methods. Therefore, some studies are currently underway to clarify their properties. One example is the insertion of continuous fibers into 3D printed parts, which has been shown to improve strength and stiffness. However, there has been little quantitative evaluation of the insertion orientation and content of continuous fiber. Especially, while the insertion position is theoretically critical to strength and stiffness, there has been no prior approach to evaluate the effect of CF layer insertion position. In this study, we quantitatively evaluated the degree of strength and stiffness improvement by inserting continuous carbon fiber into 3D printed parts during printing. To evaluate the insertion orientation, content and position, we calculated theoretical equations and discussed the discrepancy between theoretical values and experimental results. The results showed that the degree of stiffness improvement achievable in 3D printed parts was clarified in comparison with theoretical values.**

I. Introduction

The use of 3D printed parts has recently gained attention in a wide range of applications. Recent studies have shown that 3D printed parts can be used as robotic parts [1]-[3]. While 3D printed parts are often used to reduce robots' weight, certain applications, such as industrial robot arms, demand significantly higher stiffness and strength [4]. When replacing robot components with 3D printed parts, high stiffness is often required. Therefore, the strength and stiffness of 3D printed parts are considerably important. The strength and stiffness of 3D printed parts have been investigated [5]-[8]. A recent approach to enhance these properties is the use of composite materials, where some Fused Deposition Modeling (FDM) 3D printers are now capable of embedding continuous carbon fibers (CF) during the printing process. Previous research has revealed that the embedding of continuous reinforcing fibers significantly enhances the strength and stiffness of 3D printed parts [4][8]. However, it has been reported that the cost of fabrication increases with the insertion of CF [8]. Furthermore, there is little information on the effect that varying in the content and positions of CF insertion have on the strength and stiffness of 3D printed parts. Without clear design guidelines, the optimization process for 3D printed parts is complicated, potentially leading to situations where parts are overengineered or underengineered. Therefore, in this study, the changes in strength and stiffness resulting from varying in the content, orientation and position of CF insertion are evaluated.

All authors are with the Department of the Advanced Robotics, Chiba Institute of Technology, 2-17-1 Tsudanuma, Narashino, Chiba 257-0016, JAPAN
Rintaro MATSUSHITA (e-mail: s20C1107RA@s.chibakoudai.jp)
Yusuke OTA (email: yusuke.ohta@-it-chiba.ac.jp).

II. Experimental step

In this study, three-point bending experiments were conducted to compare strength and stiffness depending on the CF insertion position. The following aspects were addressed:

- **CF orientation**: The strength and stiffness change depending on the orientation of the CF inserted. Three patterns of CF orientation were prepared, and strength and stiffness were evaluated to clarify the relationship between the fiber orientation and the strength and stiffness. The CF insertion angle that produced the highest stiffness was used in subsequent experiments. (section III-A)
- **CF content and insertion position**: The stiffness of the test rod is theoretically known to change depending on the position of the CF insertion. However, it has been shown that the material properties of 3D printed parts often differ from the experimentally obtained stiffness of the final product [9]. We therefore quantitatively evaluated how much the stiffness changes based on the CF insertion position. We also compared the stiffness of reinforced test rods with that of unreinforced test rods to assess the improvement provided by the CF. The results were also compared with theoretical calculations. Considering the anisotropy of the 3D printed parts, we applied a load from two different directions relative to the laminated direction and evaluated the results. The results from the unreinforced test rod values were used as a standard value for comparison. (section III-B)
- **Adhesion between ONYX and CF layers**: The strength and stiffness of 3D printed parts are influenced not only by position and quantity of continuous fibers, but also by the quality of adhesion at material interfaces. We examined two types of interfacial adhesion, between ONYX layers and CF layers and between adjacent CF layers. (section III-C)

Test rods were modeled using 3D CAD software (Autodesk Inventor) and fabricated with the dimensions of 10×10×150

mm. As shown in Fig. 1, all test rods were printed with the Zm-axis as the lamination direction. A single condition was tested using seven samples. The infill structure and infill rate were printed using solid 100%. The laminate pitch was 0.125 mm, resulting in 80 layers.

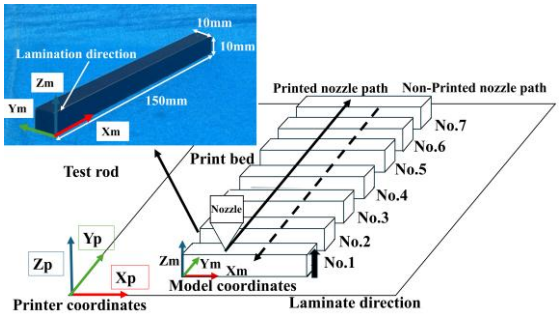

Fig. 1 Test rod printed placement

Fig. 2 shows the experimental setup and coordinate system for the three-point bending test used to measure strength and stiffness. The experiment used a force gauge (AIKOH RZE-S-200) to measure the load applied to the center of the test rod. The force gauge was moved at 10mm/min in the Ze-axis direction. The moved distance was measured by CCD Laser Displacement Transducer (KEYENCE LK-G150). Considering the anisotropy of the 3D printed parts, experiments were conducted with two loading directions, Zm and Ym, relative to the test rods, as shown in Fig. 3. The load applied perpendicular to the print bed is referred to as Zm-direction loading, while the load applied parallel to the print bed is referred to as Ym-direction loading.

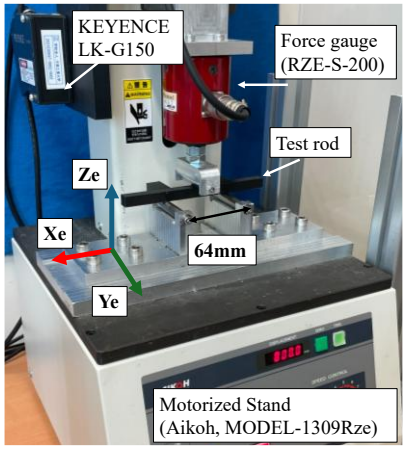

Fig. 2 Three-point bending test machine

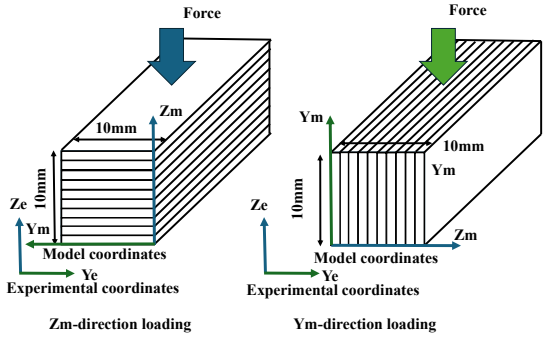

Fig. 3 Force applications direction and laminated direction

The obtained values of load and displacement were used to calculate and evaluate stress σ using equation (1) and strain ε using equation (2). The flexural modulus was calculated from the slope of the Bending stress-strain change within the range of 15% to 65% of the maximum stress as E_t [MPa], and the flexural stiffness was determined EI using equation (3). The width of the test rod is denoted as b [mm], the height as h [mm], the load as F [N], the displacement as s [mm], and the distance between supports as L [mm].

$$\sigma = \frac{3FL}{2bh^2} \tag{1}$$

$$\varepsilon = \frac{600sh}{L^2} \tag{2}$$

$$EI = E_t \frac{bh^3}{12} \tag{3}$$

III. STRENGTH AND STIFFNESS CHANGE DUE TO CF INSERTION

The changes in strength and stiffness due to CF insertion were quantitatively evaluated using three-point bending experiments. We have fabricated experimental parts using Markforged Mark Two as a 3D printer [10]. The 3D printed parts were fabricated using ONYX [11], a nylon-based material, and continuous CF [11] as a reinforcing material. The printing method employed was Fused Deposition Modeling (FDM), utilizing a 3D printer equipped with two nozzles. This setup allowed for the printing of two different materials (ONYX and CF).

A. CF orientation

To confirm the effect of CF orientation on the strength and stiffness of the 3D printed parts, three-point bending experiments were conducted. The experiments were conducted using 3D printed parts in which CF were embedded in both the top and bottom surfaces. As shown in Fig. 4, we checked the extent to which stiffness improved for three different fiber orientations from the outside of the test 3D printed parts. Due to a constraint of the 3D printer, the CF layers were inserted into the 5th layer from the top and the 5th layer from the bottom.

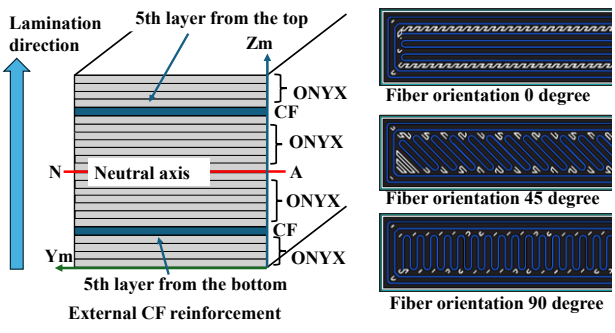

Fig. 4 CF layer insertion position and Fiber direction

Figs. 5 and 6 show the experimental results of bending stress in load direction Zm and Ym. Figs. 7 and 8 show the experimental results of stiffness in load direction Zm and Ym. The error bars in these and all subsequent Figs represent the standard deviation from seven samples.

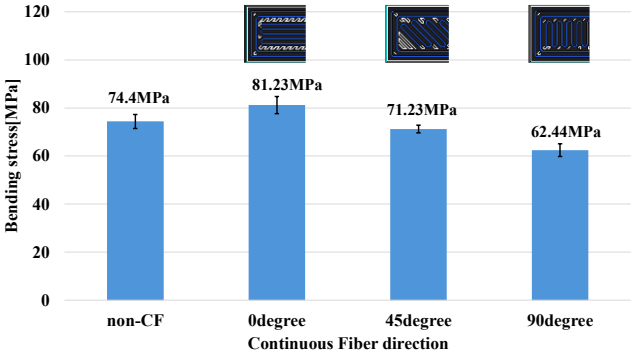

Fig. 5 Effect of CF orientation on stress for Zm-direction

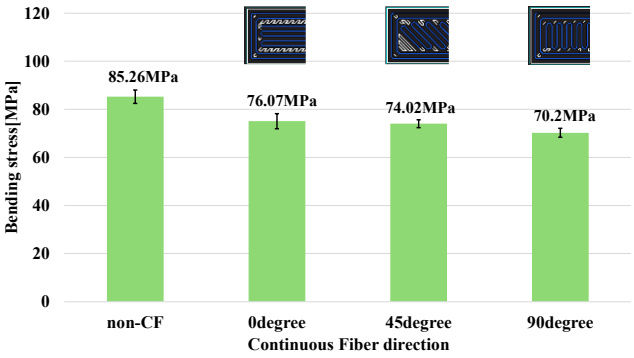

Fig. 6 Effect of CF orientation on stress for Ym-direction

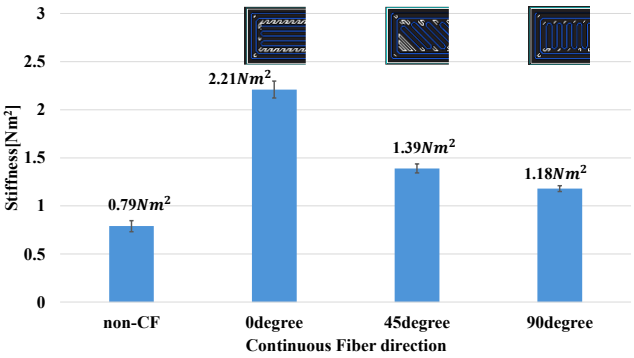

Fig. 7 Effect of CF orientation on stiffness for Zm-direction

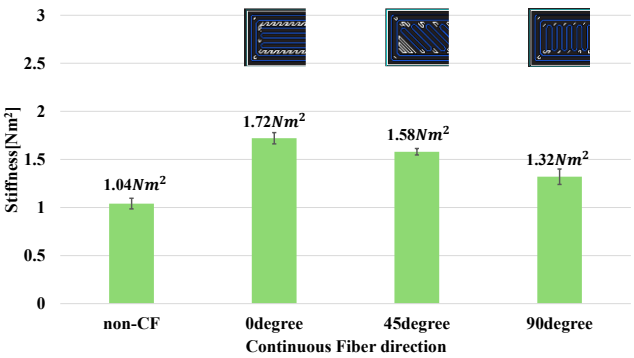

Fig. 8 Effect of CF orientation on stiffness for Ym-direction

Fig. 5 shows that the insertion of CF layers gets increased stress. In contrast, the result in Fig.6 indicated that CF layer insertion decreased in their stress. The bending stress was also found to depend on the CF orientation both Zm and Ym loads. Figs.7 and 8 also indicated that stiffness is influenced by CF orientation. Compared with the standard value, (which does not contain continuous fiber, and it is indicated as "non-CF" in Figs. 5 to 8) the stiffness improvement for the Zm-load was about 2.80, 1.76, and 1.49 times higher for the 0 degree, 45 degree and 90 degree CF orientations, respectively. For the Ym-load, the improvement was about 1.65, 1.52, and 1.27 times higher than for the same respective angles. Another important finding was that the effect of fiber orientation was more pronounced for the Zm load than for the Ym load.

We concluded that a 0 degree CF insertion orientation provides the highest stiffness in these three fiber insertion orientations. Based on this result, all subsequent experiments on the CF insertion content and position were performed using CF layers inserted at 0 degree. However, combinations of fiber orientations may also affect the variations in strength and stiffness, then these should be revealed experimentally as our future work.

B. CF content and insertion position

To confirm the Bending stress and stiffness of the 3D printed parts in the CF insertion position and content, three-point bending experiments were conducted. Fig. 9 shows the position of the CF layer inserted into the 3D printed parts and coordinate system. Two types of 3D printed parts were printed, featuring either CF inserted into the top and bottom surfaces or near the neutral axis. As shown in Fig. 9 the CF layers were inserted symmetrically with respect to the neutral axis. To evaluate the effect of varying the reinforcement quantity, 3D printed parts were printed with a total of 2, 4, 6, 8, and 10 CF layers. The direction of CF layer addition is also indicated in Fig. 9. Fig. 10 shows a cross section of the layer with CF inserted. The gaps created during CF printing were reinforced with ONYX.

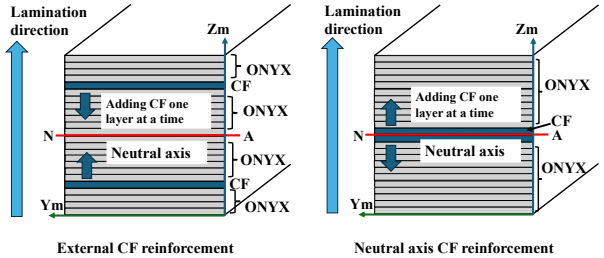

Fig. 9 Position of CF in test rod

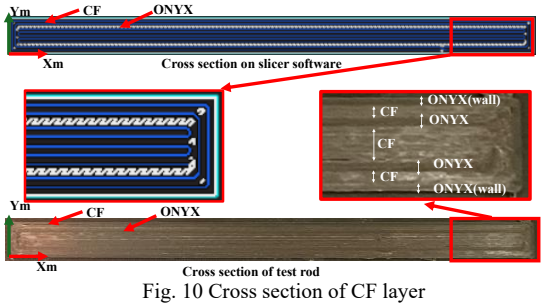

Fig. 10 Cross section of CF layer

Based on these experiments, the measured stiffness values were compared with theoretical stiffness to determine the difference between them. Since two different materials (ONYX and CF) are used in a laminated structure, the Young's modulus varies across the section, leading to different stress distributions. A theoretical value was derived for loading in the Zm direction, using the equivalent bending Young's modulus to consider the different material positions and content. However, for loading in the Ym direction, as each material is evenly positioned with respect to the neutral axis as shown in Fig. 12, a theoretical formula was used that ignores the insertion position of the materials.

It can be seen from Fig. 10 that the gaps within the CF layers are filled with ONYX, requiring the Young's modulus calculation of these layers to account for the presence of ONYX. Because of this composite effect, the theoretical Young's modulus of the CF layers was calculated using the rule of mixtures(4)(5). For Zm-direction loading, the rule of mixtures in Equation (4) is used, while for Ym-direction loading, Equation (5) is applied.

$$E_{Ocz} = \frac{E_o E_c}{V_o E_c + V_c E_o} \tag{4}$$

$$E_{Ocy} = E_o V_o + E_c V_c \tag{5}$$

Where E_o [GPa] is the bending modulus of the ONYX, E_c [GPa] is the bending modulus of the CF, V_o is the fiber volume fraction of the ONYX, and V_c is the fiber volume fraction of the CF. The values for E_o and E_c were obtained from the material properties of Markforged [11], and were used as 3.0 [GPa] and 51 [GPa], respectively. The volume fractions, V_o and V_c were calculated from the volumetric ratio of ONYX and CF within a defined layer. This ratio was determined by measuring the width of the CF during the fabrication process. According to equations (4) and (5), CF layer Young's modulus of E_{ocz} = 12.62[GPa] was used for Zm-direction loading and E_{ocy} = 41.88[GPa] was used for Ym-direction loading. The theoretical Young's modulus for the CF layers was calculated using these material properties. The theoretical calculations were performed as follows for both Zm and Ym loading directions. In addition, the theoretical adhesive conditions were used assuming perfect adhesion.

・Theoretical formula for Zm load

External CF reinforcement

$$M_x = \int_A \sigma\eta dA = 2\left(\int_0^{\frac{72-n}{160}h} \frac{E_o\eta}{\rho} b\eta d\eta + \int_{\frac{72-n}{160}h}^{\frac{9}{20}h} \frac{E_{coz}\eta}{\rho} b\eta d\eta + \int_{\frac{9}{20}h}^{\frac{h}{2}} \frac{E_o\eta}{\rho} b\eta d\eta\right)$$

$$= \frac{bh^3}{12\rho}\left(8E_o\left\{\left(\frac{72-n}{160}\right)^3 + \frac{271}{8000}\right\} + 8E_{coz}\left\{\frac{729}{8000} - \left(\frac{72-n}{160}\right)^3\right\}\right) \tag{6}$$

$$E_e = 8E_o\left\{\left(\frac{72-n}{160}\right)^3 + \frac{271}{8000}\right\} + 8E_{coz}\left\{\frac{729}{8000} - \left(\frac{72-n}{160}\right)^3\right\} \tag{7}$$

Neutral axis CF reinforcement

$$M_x = \int_A \sigma\eta dA = 2\left(\int_0^{\frac{n}{160}h} \frac{E_{coz}\eta}{\rho} b\eta d\eta + \int_{\frac{n}{160}h}^{\frac{h}{2}} \frac{E_o\eta}{\rho} b\eta d\eta\right)$$

$$= \frac{bh^3}{12\rho}\left(8E_{coz}\left\{\left(\frac{n}{160}\right)^3\right\} + 8E_o\left\{\frac{1}{8} - \left(\frac{n}{160}\right)^3\right\}\right) \tag{8}$$

$$E_n = 8E_{coz}\left\{\left(\frac{n}{160}\right)^3\right\} + 8E_o\left\{\frac{1}{8} - \left(\frac{n}{160}\right)^3\right\} \tag{9}$$

Fig. 11 indicates the distance from the neutral axis to the material transition for the two CF insertion patterns. Based on the distance from the neutral axis and the positions where the materials change, integration was performed to calculate the bending moment (6) and (8), and then equivalent Young's modulus (7) and (9) were derived.

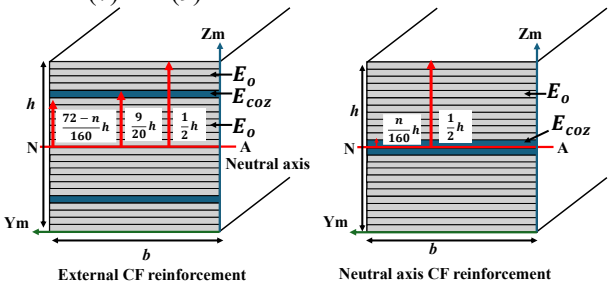

Fig. 11 Distance from neutral axis for each material

Where E_e and E_n [GPa] are the equivalent bending modulus for external and neutral axis CF insertion, respectively, η[mm] is the distance from Neutral axis, and n is the number of CF layers.

・Theoretical formula for Ym load

Ym-direction loading, a theoretical stiffness value was calculated by treating the test rod as a single homogeneous material. Fig. 12 shows the method used to calculate theoretical stiffness. In this method, the test rod is treated as a single homogeneous material by proportionally increasing the width of the CF layers based on the Young's modulus of the materials. Equation (10) is the area change equation shown in Fig. 12.

$$A'_{ocy} = \frac{E_{coy}}{E_o} A_{ocy} \tag{10}$$

Where A_{ocy} is the cross-sectional area of CF layer, and A'_{ocy} is the cross-sectional area increased in proportion to Young's modulus. The theoretical stiffness was calculated by assuming that there is no change in the value due to the difference in the CF insertion position, as the CF layers were inserted symmetrically.

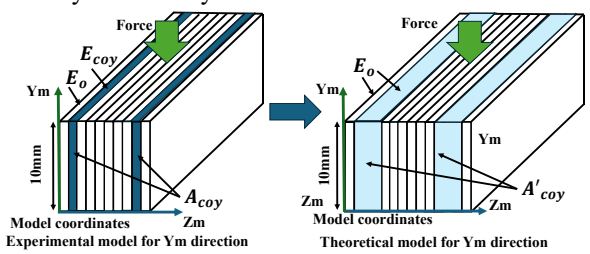

Fig. 12 Composite beam cross section

Based on these conditions, a theoretical formula considering anisotropy was derived and compared with experimental values. Figs. 13 and 14 show the experimental results of the maximum bending stress for 3D printed parts with CF inserted from the external and from the neutral axis, respectively. Figs. 15 and 16 show the experimental results of stiffness for 3D printed parts with external CF reinforcement, for the Zm and Ym loading directions, respectively. Figs. 17 and 18 show the experimental results of stiffness for 3D printed parts with neutral axis CF reinforcement, for the Zm and Ym loading directions, respectively. The theoretical stiffness values are also presented in these figures.

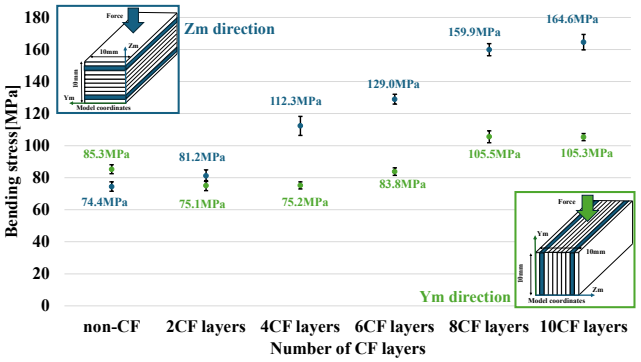

Fig. 13 Effect of external CF layer count on stress

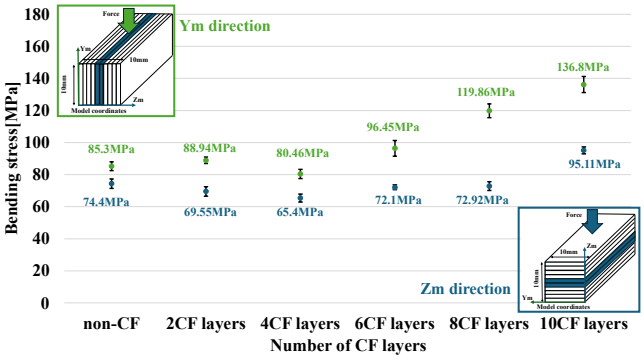

Fig. 14 Effect of neutral axis CF layer count on stress

In Fig. 13, it was confirmed that stress was increased for Zm-direction loading with the insertion of CF layers. However, for Ym-direction loading, a tendency for stress to decrease was observed. This can be attributed to the differing failure mechanisms. The unreinforced ONYX test rod exhibited ductile properties, where the stress continued to increase beyond the elastic limit. In contrast, the addition of CF layers induced brittle properties, causing the test rod to reach its maximum stress within the elastic region. However, as the number of CF layers increased, the maximum stress exceeded that of unreinforced ONYX test rod even within the elastic range, and it is thought that the maximum stress increased. The results for Zm-direction loading in Figs. 13 and 14 show that, when a load is applied to the laminate surface, a higher stress is sustained as the distance from the neutral axis increases.

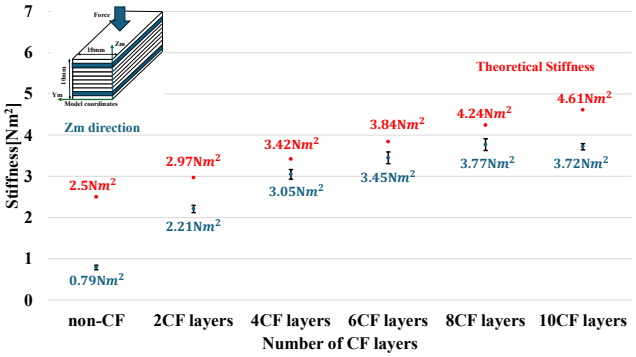

Fig. 15 Effect of external CF layer count on stiffness for Zm-direction

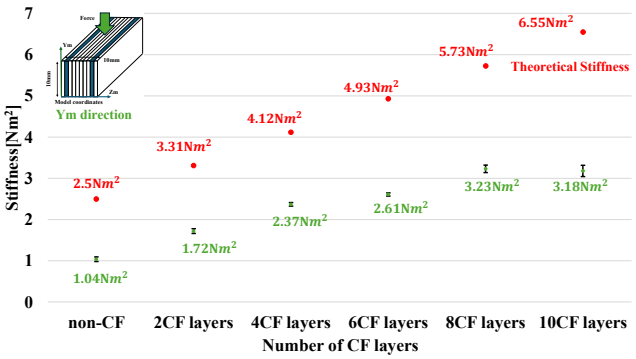

Fig. 16 Effect of external CF layer count on stiffness for Ym-direction

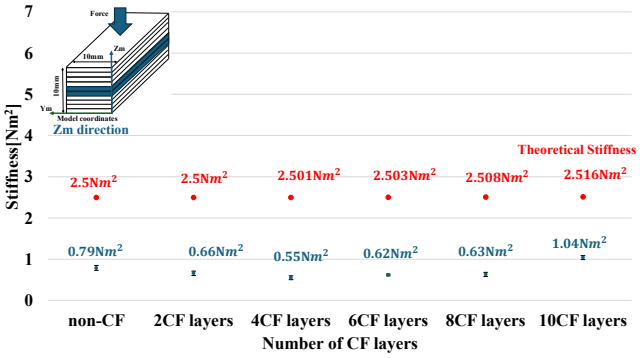

Fig. 17 Effect of neutral axis CF layer count on stiffness for Zm-direction

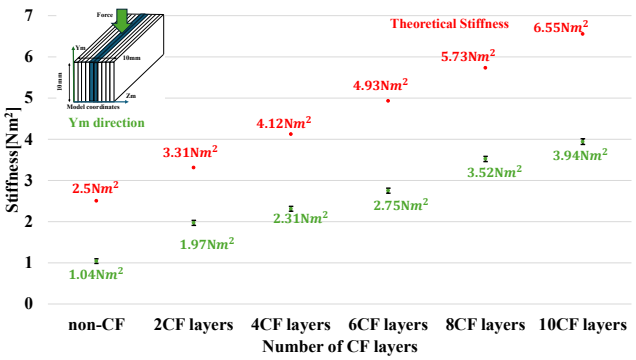

Fig. 18 Effect of neutral axis CF layer count on stiffness for Ym-direction

From Figs. 15 and 17, it was confirmed that the stiffness changes depending on the CF insertion position, which is consistent with theoretical stiffness. Specifically, from Fig.

17, it was observed that inserting CF layers near the neutral axis has little effect on improving stiffness for Zm-direction loading. Fig. 19 shows the 3D printed parts after fracture. From Fig. 19, we found that test rods with CF inserted external layers show fracture. In contrast, fracture is less noticeable in the CF regions closer to the neutral axis. This indicates that even if the content of CF inserted is the same, the insertion position determines whether test rods have brittle or ductile properties. In addition, comparing strength and stiffness when inserting CF on the external and on the neutral axis side, it was shown that inserting CF layers on the external is a more cost effective method to increase strength and stiffness. This suggests that, when considering part costs, it is necessary to reinforce with CF only in the areas required to maintain stiffness. From Figs. 16 and 18, it was confirmed that for Ym-direction loading, the change in stiffness due to the position of the CF layers is small, and the experimental stiffness is approximately 50-60% of the theoretical value. This indicates that when considering stiffness for Ym-direction loading, the position of the CF layers is less critical. However, there is a large discrepancy from the theoretical value, and when a load is applied between layers, such as the Ym load, it is thought that the adhesive conditions between the layers must be taken into consideration. In summary, stiffness under the Zm load is dominated by the CF insertion position, while this effect is minimal for the Ym load. This implies that position is a key design factor for the Zm load, but not for the Ym load.

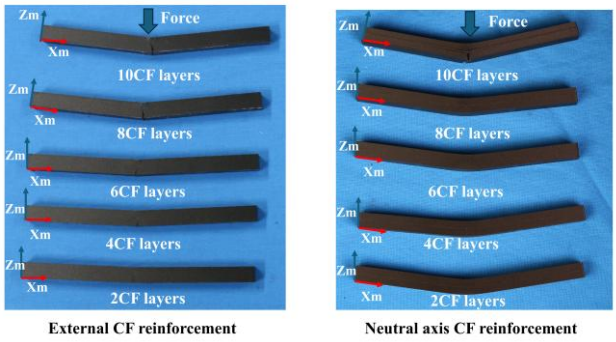

Fig. 19 Fracture test rods for Zm-direction

C. *Adhesion between ONYX and CF layers*

To confirm the strength and stiffness between layers of different materials in 3D printed parts, we used test rods with CF inserted from the external, as in the previous experiment. Fig. 20 shows that when adding multiple CF layers, inserting an ONYX layer between them increases the number of adhesive layers between the CF and ONYX layers. Like the pattern of external CF insertion shown in Fig. 9, we added CF layers in increments of two and compared the strength and stiffness up to a final count of 10 layers. Zm-direction load stiffness was compared with theoretical stiffness to consider the insertion position of CF layers. Fig. 21 shows the bending stress results, while Figs. 22 and 23 illustrate the stiffness for Zm and Ym loads. Table I shows the percentage of stiffness relative to theoretical stiffness corresponding to Figs. 15,16 and Table II show the percentage of stiffness relative to theoretical stiffness corresponding to Figs. 22 and 23. According to Table I and II, the ratios of measured stiffness to theoretical stiffness for Zm load, Ym load, and each number of CF layers are in close agreement. From the results, we found that an increase in the number of CF alternating layers has a minimal impact on the overall stiffness.

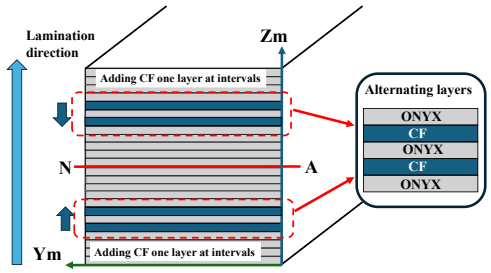

Fig. 20 Position of carbon fiber in test rods with alternating layers

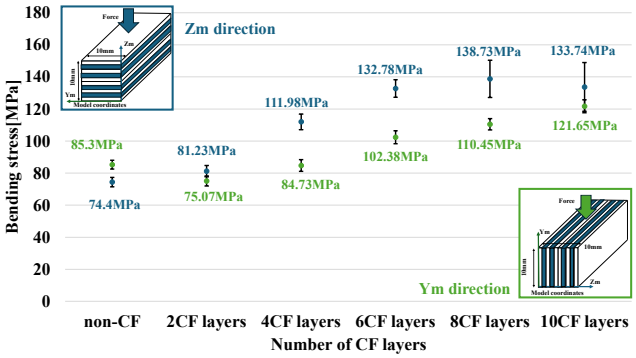

Fig. 21 Effect of alternating external CF and onyx layers on stress

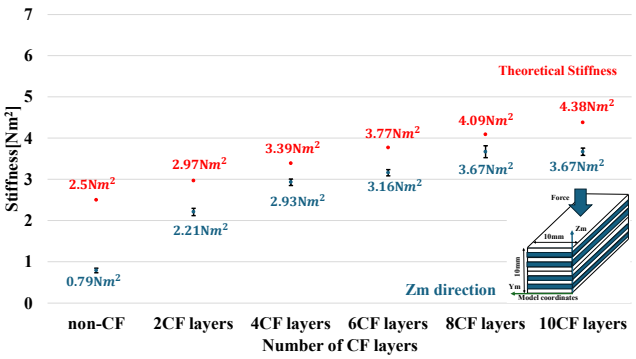

Fig. 22 Stiffness of alternating external layers for Zm-direction

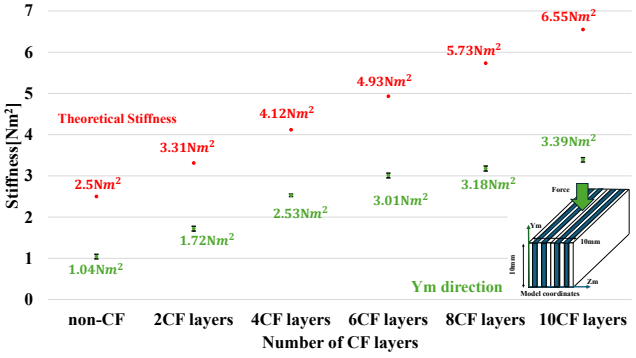

Fig. 23 Stiffness of alternating external layers for Ym-direction

TABLE I
Comparison of measured and theoretical stiffness for external CF

Number of CF layers	Zm-direction loading[%]	Ym-direction loading[%]
4 CF layers	89.18	57.52
6 CF layers	89.84	52.94
8 CF layers	88.92	56.37
10 CF layers	80.69	48.55

TABLE II
Comparison of measured and theoretical stiffness for external CF alternating

Number of CF layers	Zm-direction loading[%]	Ym-direction loading[%]
4 CF layers	86.43	61.41
6 CF layers	83.82	61.05
8 CF layers	89.73	55.50
10 CF layers	83.79	51.76

IV. CONCLUSION

In this study, the effects of the CF layers insertion orientation, content and position on strength and stiffness were evaluated to propose optimal design methodology for 3D printed parts. First, the effect of the CF insertion orientation on strength and stiffness was evaluated. Three types of 3D printed parts with different CF orientations were printed and tested for Zm and Ym loads. The result showed that the orientation is a critical factor, particularly for the stiffness in the Zm load, which varied by a factor of about1.8, while the variation in the Ym load was a factor of about 1.3. Then, using the fiber orientation that yields the highest stiffness in the previous test, three-point bending experiments were conducted to evaluate the effect of the CF content and insertion position. For the Zm load, test rods with external CF reinforcement achieved stiffness of about 75-90% of the theoretical stiffness. In contrast, for test rods reinforced near the neutral axis, increasing the number of CF layers had not improved its stiffness. For the Ym load, however, no significant difference was observed between the insertion positions; the stiffness was around 50% of the theoretical stiffness in both cases. Additionally, strength and stiffness between the layers of different materials in the 3D printed parts were evaluated. As a result, it was determined that the overall stiffness was largely independent of the number of different material interfaces. From these findings, it was confirmed that the Ym load does not depend on the interface where different materials are adjacent or the insertion position of the CF and shows approximately 50% of the theoretical stiffness. Based on these findings, we will continue to investigate further whether this discrepancy depends on the adhesion conditions. Finally, we believe that understanding the empirical performance of 3D printed parts as structural components, as demonstrated in this study, provides engineers with practical design values. Utilizing these values can significantly reduce the risks of both overengineering and underengineering.

In the future, we will investigate strength and stiffness evaluation by infill structure, we will increase the number of samples. We also aim to develop a simplified stiffness prediction formula for 3D printed parts, contributing to the optimal design.

.

ACKNOWLEDGMENT

This paper is an achievement of joint research with and is jointly owned copyrighted material of ROBOT Industrial Basic Technology Collaborative Innovation Partnership. And this paper is also based on results obtained from a project, JPNP14004, commissioned by the New Energy and Industrial Technology Development Organization (NEDO). Finally, we thank Prof. Gen Endo (Institute of Science Tokyo), Prof. Naoyuki Takesue (Tokyo Metropolitan University), and Prof. Takeshi Takaki (Hiroshima University) for their valuable comments and discussion.

REFERENCES

[1] Y. Bao and T. Takaki, "Estimation of the 3D printing filling density effect on natural frequency and damping ratio and the optimal filling density of robot structure," *2025 IEEE/SICE International Symposium on System Integration (SII)*, Munich, Germany, 2025, pp. 303-308

[2] H. Satake and N. Takesue, "Comparison of Characteristics of Cycloidal Gear Reducer of 20 Different Combinations of Metal and Plastic Parts," *2025 IEEE/SICE International Symposium on System Integration (SII)*, Munich, Germany, 2025, pp. 309-314

[3] S. Mukherjee and T. Takaki, "A Data-driven Comparison of Resistive-Viscoelastic Models for a 3D-Printed Conductive Solid," *2025 IEEE/SICE International Symposium on System Integration (SII)*, Munich, Germany, 2025, pp. 326-331

[4] N. Takesue, K. Sugihara, G. Endo, Y. Tsukamoto and T. Takaki, "Stiffness Measurement and Modeling of Robot Arm Consisting of Single Geared Joint and Link Made of Different Materials," *2025 IEEE/SICE International Symposium on System Integration (SII)*, Munich, Germany, 2025, pp. 315-319

[5] R. Matsushita and Y. Ota, "Stiffness and Strength Changes of 3D Printed Parts due to Bonding," *2025 IEEE/SICE International Symposium on System Integration (SII)*, Munich, Germany, 2025, pp. 339-344

[6] K. Osawa and G. Endo, "Does Thin-Walled Metal Pipe Insertion Increase the Bending Strength of 3D Printed Parts?," *2024 IEEE/SICE International Symposium on System Integration (SII)*, Ha Long, Vietnam, 2024, pp. 585-591

[7] N. Kanai, H. Nabae and G. Endo, "Empirical Strength Comparison of 3D printed Beams and Proposal of a Joining Method for Large Parts*," *2025 IEEE/SICE International Symposium on System Integration (SII)*, Munich, Germany, 2025, pp. 332-338

[8] T Takaki, “Fastening of plastic parts produced by fused-deposition modeling 3D-printer with machine key” “ROBOMECH, 1A1-I16,2023, Nagoya, Aichi.

[9] R. Matsushita and Y. Ota, "Stiffness and Strength Changes of 3D Printed Parts due to insert continuous fiber,"2025 The Robotics Society of Japan (RSJ), Oookayama, Japan, 2025,

[10] https://www-objects.markforged.com/craft/3d_printers_detail/mark-two/F-PR-2027.pdf/Accessed:November,13,2025

[11] https://web-objects.markforged.com/craft/materials/CompositesV5.2.pdf?_gl=1*7nnrun*_gcl_au*MTE2NTM5MTA4My4xNzQ2NjE0MTU5/Accessed: Jun,22,2025